Inorganic Chemistry

Communication

pubs.acs.org/IC

Versatile Mesoporous Dy^{III} Coordination Framework for Highly Efficient Trapping of Diverse Pollutants

Miao Du,*[,†] Min Chen,[‡] Xi Wang,[†] Jiong Wen,[‡] Xiao-Gang Yang,[‡] Shao-Ming Fang,[‡] and Chun-Sen Liu*[,‡]

[†]College of Chemistry, Tianjin Key Laboratory of Structure and Performance for Functional Molecules, MOE Key Laboratory of Inorganic−Organic Hybrid Functional Material Chemistry, Tianjin Normal University, Tianjin 300387, P. R. China

[‡]Henan Provincial Key Lab of Surface & Interface Science, Zhengzhou University of Light Industry, Zhengzhou, 450002 Henan, P. R. China

Supporting Information

ABSTRACT: This work presents a mesoporous Dy^{III} metal−organic framework with two types of void cages (diameters: 4.4 and 2.8 nm), which can efficiently adsorb a variety of chemical pollutants, including toxic metals, iodine, and formaldehyde.

As a result of rapid industrial development, environmental pollution has become a big threat to the ecological environment and human health.[1] The familiar chemical pollutants comprise toxic metals,[2a] radioactive nuclear wastes,[2b] volatile organic compounds, etc.[2c] The most widely used approach to removing such chemical pollutants is adsorption.[3] Thus, the development of new porous materials for highly efficient adsorption of pollutants is of great significance. In this context, a variety of porous materials such as activated carbon,[4a] zeolite,[4b] resin,[4c] and membrane[4d] have been extensively explored.

Metal−organic frameworks (MOFs) are an emerging class of inorganic−organic hybrid porous materials.[5] Compared with conventional adsorbents, the advantages of MOFs lie in their permanent porosity, high surface areas, and especially tunable pore sizes and properties.[6] Although the applications of MOFs in pollutant trapping have been investigated, the development of high-performance materials with versatile sorption capacities represents one of the greatest challenges.[7] Moreover, most known MOFs just have micropores (pore size <2 nm), which clearly cannot meet those demands for holding larger guests.[8] Thus, the design and synthesis of mesoporous MOFs (mesoMOFs, pore size = 2−50 nm) will be imperative, which, however, are very difficult in practice.[9] As a result, no more than 100 mesoMOFs have been known so far, among which only one case is lanthanide-based (see Table S10 in the Supporting Information, SI). Herein, we will report a unique Dy^{III} mesoMOF material (438-MOF), which has a broad spectrum of sorption capacity toward different chemical pollutants. Significantly, 438-MOF can be used as the stationary phase of a chromatographic column for fast metal separation and exchange.

Solvothermal reaction of $Dy(NO_3)_3{\cdot}6H_2O$ and 4,4′,4″-*s*-triazine-1,3,5-triyltri-*p*-aminobenzoic acid (H_3TATAB) in *N*-methyl-2-pyrrolidone (NMP) produces colorless block crystals of $\{[Dy_3(TATAB)(H_2O)_6](NO_3)_6(NMP)_{17}(H_2O)_5\}_n$ (438-MOF; see the SI for details). Single-crystal X-ray diffraction analysis reveals that 438-MOF crystallizes in the cubic system with space group $I\bar{4}3m$ with a very large unit cell volume of 61743(2) Å^3, which has a (4,24)-connected **twf**-type[10] network based on superoctahedron (SO). The structure is constructed by mixing octahedral (Dy_3) and square-paddlewheel (Dy_2) secondary building units (SBUs), which are linked to six and four TATAB ligands, respectively (Figure S3a,b in the SI). Generally, Ln^{III} metal ions will take higher coordination numbers (7−10), while in the Dy_3 SBU here, each Dy^{III} center adopts a rare hexacoordinated sphere, which should result from the steric crowding of six larger TATAB ligands around each SBU.

The overall 3D framework results from the linkages of two types of microporous and mesoporous cages (Figure 1). Each TATAB ligand is connected to one Dy_2 and two Dy_3 SBUs (Figure S3c in the SI), forming a microporous SO cage (see Figures 1a and S4 in the SI) with an inner-sphere diameter of 1.4 nm, measured by fitting a sphere from the centroid of each cage to the van der Waals surface of its walls. In each SO, four Dy_3 SBUs are located in the equatorial plane and the axial positions are occupied by two Dy_2 SBUs. Four of eight faces are spanned by the TATAB ligands, and the other four open faces act as windows with an aperture of ca. 1.2 nm (see Figure S5 in the SI). Furthermore, 24 such microporous SO cages are assembled in an edge-sharing fashion to define a mesoporous cage, with an inner-sphere diameter of 2.3 nm and an overall edge length of 4.4 nm (Figures 1b and S6 in the SI). The window size of each mesoporous cage is the same as that of the microporous cage (Figures S7 and S8 in the SI). The effective free volume for the framework is as large as 46387.3 Å^3 (75.1% per unit cell volume).

The underlying topology[11] for 438-MOF can be ascribed to a unique (4,24)-connected **twf** network, in which each microporous cage shares its windows with four mesoporous cages and each mesoporous cage is surrounded by 24 microporous ones (see Figure 1c−e). The connectivity of the **twf** net can also be described by the tiles of **twf-d** (dual structure of **twf**). The inner voids of two types of cages equate to the natural tiling of $[6^4]$ and $[6^{24}]$ in the **twf-d** net, respectively. As a result, a (4,24)-connected **twf** net can be obtained by placing the vertex in the tiles of $[6^4]$ and $[6^{24}]$ and linking these new vertices by edges

Received: March 9, 2014
Published: July 2, 2014

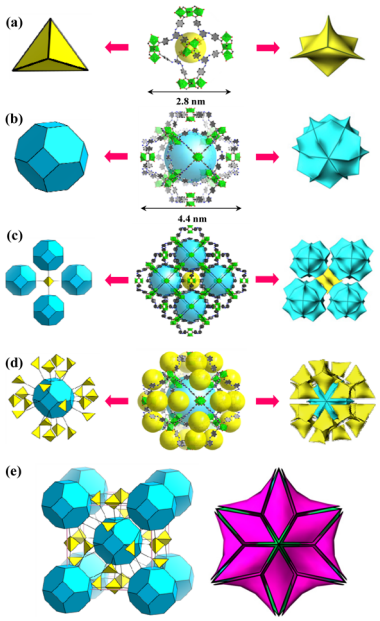

Figure 1. (a and c) 4-Connected microporous cage and (b and d) 24-connected mesoporous cage. (left) Polyhedron and (right) natural tiling (yellow and cyan for natural tiling of [6^4] and [6^{24}]) correspond to the vertices. (e) (left) Augmented version and (right) natural tiling of the (4,24)-connected **twf** network for 438-MOF.

passing through the faces of two tiles.[10] On the other hand, considering the $Dy_3(CO_2)_6$ and $Dy_2(CO_2)_4$ motifs as the octahedron and square inorganic SBUs and the TATAB ligand as the organic triangle SBU, an augmented (3,4,6)-connected **twf-d** net (Figure S9 in the SI) can also be constructed.

The thermogravimetric analysis (TGA) curve of as-synthesized 438-MOF reveals that the framework can be stable up to ca. 400 °C (see Figure S2 in the SI). However, the powder X-ray diffraction (PXRD) pattern shows that 438-MOF will lose its crystallinity upon heating to 100 °C, which, as expected, has no N_2 adsorption. Thus, the supercritical carbon dioxide drying (SCD) method was used for sample activation of 438-MOF, which will retain its crystallinity (Figure S10 in the SI) and exhibit a type IV sorption isotherm with a Brunauer–Emmett–Teller specific surface area of 946 $m^2\ g^{-1}$ and an N_2 sorption of 742 $cm^3\ g^{-1}$ (Figure S11 in the SI). Notably, the sample after SCD treatment still holds ca. 25% solvents (Figure S12 in the SI).

The large cage voids with nanoscale open windows for 438-MOF make it feasible to capture and further separate different pollutants. First, the response of a single-metal ion to 438-MOF was tested. When a single crystal of 438-MOF was dipped into a $Cu(NO_3)_2$ solution, a gradual color change (from colorless to green) was observed, occurring from the surface to the center of the crystal (see Figure S13 and Video S1 in the SI). The color of the Cu@438-MOF crystal was retained after it was washed with fresh solvents several times. Similar color changes were also observed for other metals, and then the trapping capacity for a single-metal ion was evaluated by inductively coupled plasma mass spectrometry (ICP-MS), which reveals that 438-MOF has higher uptakes for Fe^{3+}, Cu^{2+}, Hg^{2+}, and MnO_4^-, with the molar ratios of metal/Dy^{III} of 2.91/1, 2.24/1, 2.18/1, and 2.07/1, respectively (see Figure 2a and Table S3 in the SI). In addition, the sorption of different metals in 438-MOF crystals with structural integrity can be confirmed by IR and PXRD patterns (Figures S14 and S15 in the SI). The selectivity for 438-MOF, after treatment in a mixture solution of two equivalent metals,

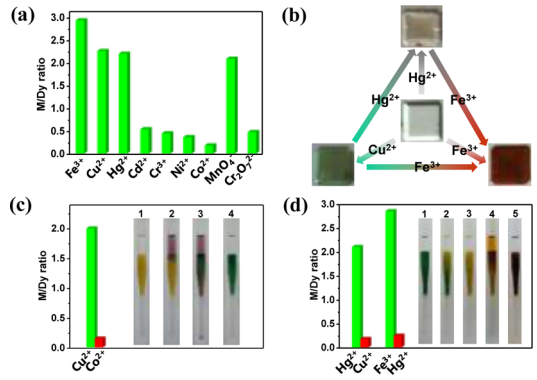

Figure 2. (a) ICP-MS analysis of metal contents (as M/Dy) for 438-MOF after metal sorption. (b) Crystal transformations for 438-MOF and Cu^{2+}, Hg^{2+}, or Fe^{3+} including 438-MOF. (c) Selectivity and column-chromatographic separation process for a Cu^{2+}/Co^{2+} mixture. (d) Selectivity and column-chromatographic exchange process for Cu^{2+}/Hg^{2+} and Hg^{2+}/Fe^{3+} mixtures.

was also determined by ICP-MS (Table S4 in the SI). Interestingly, 438-MOF has higher adsorption selectivity for Fe^{3+}/Hg^{2+} (11.56/1) and Hg^{2+}/Cu^{2+} (11.78/1), although the sorption amounts for these single-metal ions are similar. As a result, crystal transformations (Figure 2b) between Cu/Hg/Fe@438-MOF can be readily completed in minutes (Figures S16–S18 and Videos S2–S4 in the SI). Moreover, the higher selectivity of 438-MOF for Cu^{2+}/Co^{2+} (13.31/1), with similar sizes and masses and the same valence state, also reveals the extreme sensitivity of such an adsorption process.

Inspired by its higher sorption selectivity and fast delivery for diverse metals, a chromatographic column with 438-MOF as the stationary phase (40 mm × 5 mm; column 1 in Figure 2c) was produced for their separation and exchange. A mixing solution of Cu^{2+}/Co^{2+} can be successfully separated by passing it through the 438-MOF-filled column (columns 2 and 3 in Figure 2c and Video S5 in the SI), and Cu^{2+} will be retained after three times of elution by free solvent (column 4 in Figure 2c). Of further interest, when the eluting agent of a saturated $Hg(NO_3)_2$ solution was added to the Cu@438-MOF-filled column, the Cu^{2+} species can be gradually exchanged along with the $Hg(NO_3)_2$ stream (columns 1–3 in Figure 2d). Further, the Hg@438-MOF-filled column can be similarly replaced by a $Fe(NO_3)_3$ solution with a clear color change from yellow to reddish-brown (columns 4 and 5 in Figure 2d). The stepwise color changes of the column suggest that Cu^{2+} can be easily replaced by Hg^{2+} and then by Fe^{3+}. So far, there have been quite limited reports on ion separation with MOF materials,[12,13] especially their application in chromatography.[13] To the best of our knowledge, this work represents the first realization of MOF column chromatography for ion exchange.

Also, 438-MOF has highly efficient sorption of iodine, which may be applied to remove the radioactive nuclear waste (^{129}I). When a powder sample of 438-MOF and I_2 crystals were placed in a closed system at room temperature [$p(I_2)$ = ca. 0.3 Torr], a gradual color change of 438-MOF (from off-white to dark brown) was found within 1 day (Figure 3a). I_2 inclusion can also be achieved by dipping the 438-MOF crystals into a saturated cyclohexane solution of I_2, where the form and size of the single crystal are unchanged while the color will be intensified from colorless to black (see Figure 3b). The I_2 inclusion starts at the crystal surface and then diffuses into the central section, which is similar to the adsorption processes of metals. When a fresh

dx.doi.org/10.1021/ic5005374 | Inorg. Chem. 2014, 53, 7074–7076

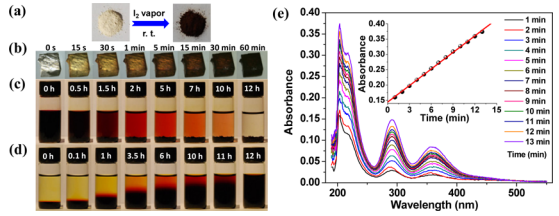

Figure 3. (a) 438-MOF sample before and after I_2 vapor sorption. (b) Single crystal of 438-MOF soaked in a I_2 solution. (c) Bulk 438-MOF sample in a I_2 solution. (d) I_2@438-MOF in dry ethanol. (e) UV/vis spectra of I_2@438-MOF for the release process of I_2.

sample of 438-MOF (ca. 150 mg) is immersed in a I_2 solution, the dark-brown solution fades to colorless by degrees (Figure 3c). Such a I_2 sorption is reversible, and the trapped I_2 can be easily removed from the sample. When the crystals of I_2@438-MOF are soaked in dry ethanol, the color of the solution deepens gradually from light yellow to dark brown, showing the release of I_2 molecules from the sample (Figure 3d). This process can also be confirmed by UV/vis spectra (Figure 3e). Further, thiosulfate determination of the I_2 content released from I_2@438-MOF shows an uptake of 0.85 g of I_2/1 g of 438-MOF, which is one of the highest I_2 sorption quantities reported to date.[14]

Formaldehyde is a very common pollutant in our daily life. Activated carbon is the most effective adsorbent for removing HCHO, while the related application with MOFs is surprisingly unknown so far. In comparison, we monitored formaldehyde adsorption of 438-MOF and activated carbon in a closed system of HCHO vapor (see Figure S20 in the SI), measured by an iodometric method (see the SI). The sorption of HCHO for 438-MOF proceeds with a rapid burst (from the first to fifth days), until a constant maximum amount (0.22 g of HCHO/1 g of 438-MOF) is achieved (Figure 4a). However, the HCHO uptake

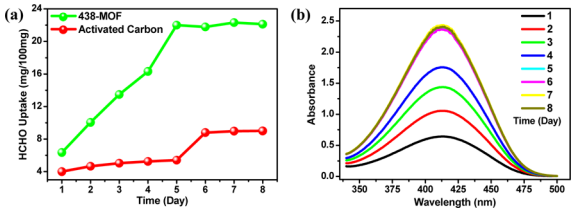

Figure 4. (a) Time-independent HCHO uptakes with 438-MOF and activated carbon materials. (b) UV/vis determination of the HCHO content in HCHO@438-MOF.

increases gradually and slowly for activated carbon (from the first to fifth days). Notably, an abrupt rise of the HCHO uptake is observed in the sixth day, and after that, the maximum amount remains constant to 0.09 g of HCHO/1 g of activated carbon. Notably, this explosion should be properly attributed to the sorption of abundant water by activated carbon (see Figure S21 in the SI for the wet sample), where HCHO can be dissolved. Anyway, the fast and abundant sorption of HCHO for 438-MOF shows its great potential for applications. The HCHO sorption for 438-MOF has also been determined by an acetylacetone spectrophotometric method (Figures 4b and S22 in the SI), which is similar to the result of the iodometric method.

In summary, a mesoporous Dy^{III} 438-MOF based on a trigonal carboxylate building block has been successfully synthesized in gram scale with high yield, which displays the (4,24)-connected **twf** network and, remarkably, highly efficient trapping capability for a variety of pollutants. The results will provide further opportunity of MOF materials for different targeted applications in environmental conservation and related scopes.

■ ASSOCIATED CONTENT

Supporting Information

Experimental details, TGA and PXRD plots, crystal structures, IR and UV/vis spectra, N_2 sorption, metal capture and exchange (crystal photos and videos), I_2 and HCHO sorption, and crystallographic data (CIF). This material is available free of charge via the Internet at http://pubs.acs.org.

■ AUTHOR INFORMATION

Corresponding Authors

*E-mail: dumiao@public.tpt.tj.cn.
*E-mail: chunsenliu@zzuli.edu.cn.

Notes

The authors declare no competing financial interest.

■ ACKNOWLEDGMENTS

This work was supported by the National Natural Science Foundation of China (Grants 21031002, 91122005, 21171151, and 21201154), Plan for Scientific Innovation Talent of Henan Province, Program for New Century Excellent Talents in University of China (Grant NCET-10-0143), and Program for Innovative Research Team in University of Tianjin (Grant TD12-5038).

■ REFERENCES

(1) Hill, M. K. *Understanding Environmental Pollution*; Cambridge University Press: Cambridge, U.K., 2010.
(2) (a) Singh, V. P. *Toxic Metals and Environmental Issues*; Sarup & Sons: New Delhi, India, 2005. (b) Ojovan, M. I.; Lee, W. E. *An Introduction to Nuclear Waste Immobilisation*; Elsevier Ltd.: Oxford, U.K., 2005. (c) Koppmann, R. *Volatile Organic Compounds in the Atmosphere*; Blackwell Publishing Ltd.: Oxford, U.K., 2007.
(3) Crini, G.; Badot, P.-M. *Sorption Processes and Pollution*; Presses University de Franche-Comté: Besançon, France, 2010.
(4) (a) Bandosz, T. J. *Activated Carbon Surfaces in Environmental Remediation*; Elsevier Ltd.: Oxford, U.K., 2006. (b) Kulprathipanja, S. *Zeolites in Industrial Separation and Catalysis*; Wiley-VCH Verlag GmbH & Co. KGaA: Weinheim, Germany, 2010. (c) Acton, Q. A. *Ion Exchange Resins: Advances in Research and Application*; Scholarly Editors: Atlanta, GA, 2012. (d) Tanaka, Y. *Ion Exchange Membranes*; Elsevier Ltd.: Oxford, U.K., 2007.
(5) Furukawa, H.; Cordova, K. E.; O'Keeffe, M.; Yaghi, O. M. *Science* **2013**, *341*, 1230444.
(6) Farha, O. K.; Hupp, J. T. *Acc. Chem. Res.* **2010**, *43*, 1166−1175.
(7) Khan, N. A.; Hasan, Z.; Jhung, S. H. *J. Hazard. Mater.* **2013**, *244*−*245*, 444−456.
(8) Fang, Q.-R.; Makal, T. A.; Young, M. D.; Zhou, H.-C. *Comments Inorg. Chem.* **2010**, *31*, 165−195.
(9) Xuan, W.; Zhu, C.; Liu, Y.; Cui, Y. *Chem. Soc. Rev.* **2012**, *41*, 1677−1695.
(10) Delgado-Friedrichs, O.; O'Keeffe, M.; Yaghi, O. M. *Acta Crystallogr., Sect. A: Found. Crystallogr.* **2006**, *62*, 350−355.
(11) O'Keeffe, M.; Yaghi, O. M. *Chem. Rev.* **2012**, *112*, 675−702.
(12) (a) Fei, H.; Rogow, D. L.; Oliver, S. R. J. *J. Am. Chem. Soc.* **2010**, *132*, 7202−7209. (b) Jiang, H.-L.; Tatsu, Y.; Lu, Z.-H.; Xu, Q. *J. Am. Chem. Soc.* **2010**, *132*, 5586−5587. (c) Zhao, X.; Bu, X.-H.; Wu, T.; Zheng, S.-T.; Wang, L.; Feng, P.-Y. *Nat. Commun.* **2013**, *3*, 3344.
(13) Lan, Y.-Q.; Jiang, H.-L.; Li, S.-L.; Xu, Q. *Adv. Mater.* **2011**, *23*, 5015−5020.
(14) Zeng, M.-H.; Wang, Q.-X.; Tan, Y.-X.; Hu, S.; Zhao, H.-X.; Long, L.-S.; Kurmoo, M. *J. Am. Chem. Soc.* **2010**, *132*, 2561−2563.